Design and additive manufacturing of closed cells from supportless lattice structure

Additive Manufacturing 33 (2020) 101168

Contents lists available at ScienceDirect

Additive Manufacturing

journal homepage: www.elsevier.com/locate/addma

Design and additive manufacturing of closed cells from supportless lattice structure

Ajeet Kumar[a,b], Luca Collini[c], Alix Daurel[a], Jeng-Ywan Jeng[a,b,*]

[a] High Speed 3D Printing Research Center, National Taiwan University of Science and Technology, No. 43, Sec. 4, Keelung Rd, Taipei, 106, Taiwan, ROC
[b] Department of Mechanical Engineering, National Taiwan University of Science and Technology, No. 43, Sec. 4, Keelung Rd, Taipei, 106, Taiwan, ROC
[c] Department of Engineering and Architecture, University of Parma, Parco Area delle Scienze 181/A, 43124, Parma, Italy

ARTICLE INFO

Keywords:
Additive manufacturing
Material extrusion process
Cellular lattice structures
Support-less lattice structure
Closed cell lattice structure

ABSTRACT

In nature, mesoscopic or microscopic cellular structures like trabecular bone, wood, shell, and sea urchin, can have high load-carrying capacity. These cellular structures with diverse shapes, forms and designs can be mainly classified into open and closed cell cellular structures. It is difficult to replicate these natural complex lattice structures with traditional manufacturing, but additive manufacturing (AM) technology development has allowed engineers and scientists to mimic these natural structures. Fabricating close cell lattice structures is still considered difficult due to the support structure within the lattices. This paper evaluates a novel way of fabricating a close cell lattice structure with a material extrusion process. The design eliminates the need for support structures and the subsequent post-processing required to remove them. A shell-shaped close cell lattice structure bio-mimicking a sea urchin shape was introduced for the load-bearing structure application. The mechanical properties of the proposed structure, including stiffness, deformation behavior and energy absorption, were compared with those of benchmarked honeycomb and open cell sea urchin (SU) lattice structures of the same density. SU lattice structures and honeycomb periodic lattice structures with varied sizes but the same morphology and fixed density were designed and printed in polylactic acid material (PLA). Their physical characteristics, deformation behavior, and compressive properties were investigated experimentally and via finite element analysis. The effect of the unit cell size on mechanical properties was studied and discussed, and the rankings of better performances were drawn. A possible application of the closed cell is for fabricating the load bearing structure; it can also be encapsulated within a fluid to impart strength and damping characteristics.

1. Introduction

Enhancing the load-bearing capabilities of an additive manufactured structure can be done in several ways by modifying the material or modifying the manufacturing process. However, these are all associated with a high cost. Designing a lattice structure to improve the load-bearing and energy absorption capabilities of additive manufactured components is more efficient, but this requires a multidisciplinary approach. Load-bearing structures are used in the biomedical, automotive, space, civil engineering, and other fields. Scientists and engineers have taken inspiration from nature because nature designs extremely appropriate cellular structure morphologies based on the surroundings. Natural structures have been developed over long-term adaptive evolution, and they are structurally and functionally optimized because natural economy is directly related to saving material and energy [1–4]. Hence, the use of cellular structures is not casual.

A lattice disposition can produce a stiff, strong load-bearing structure using as little material as possible. Natural topologies and lattice structures have been studied extensively to make man-made structures efficient in terms of material and energy without compromising on functional needs [5]. Some of the topologies like spider webs are very lightweight while also exhibiting very high load carrying capacities [6]. The honeycomb two-dimensional prismatic lattice structure has dominated engineering cellular materials in many application over two decades [7]. Foams like trabecular bone, cork, and sea shell are examples of three-dimensional cellular structures that have recently been extensively replicated and analyzed [8,9].

Cellular structures are made up of an interconnected network of plates or solid struts. When there is a repeating pattern to a cellular

* Corresponding author at: High Speed 3D Printing Research Center, National Taiwan University of Science and Technology, No. 43, Sec. 4, Keelung Rd, Taipei, 106, Taiwan, ROC.
E-mail address: jeng@mail.ntust.edu.tw (J.-Y. Jeng).

https://doi.org/10.1016/j.addma.2020.101168
Received 2 January 2020; Received in revised form 13 March 2020; Accepted 14 March 2020
Available online 19 March 2020
2214-8604/

structure, it is typically referred as a "lattice structure" [10–12]. All these natural cellular structures can be divided into two different types: a) open cell cellular structure, or b) closed cell cellular structure. Cork, balsa wood, and leaves have closed cell structures, whereas a bone has an open cell structure. The design of closed cells is more complicated than that of open cells. Closed cells can be designed using two principles: 1) the main mechanical properties can be derived entirely from cell edges or surfaces identical to an open cell lattice structure, and thin solid membranes close off the cell faces; 2) a substantial fraction of solid is at the faces of the cell and not at the edges. In this case, the cell face contributes the dominant mechanical property instead of the cell edge, as explained in the first type [13]. Natural materials like leaves have this morphology; also, some of the polymers and glasses contribute a substantial fraction of the solid at the faces and not at the edges [10]. Closed cell cellular structures can further be designed as global closed cell cellular structures or local closed cellular structures. In a global closed cell cellular structure, an open cell cellular structure is enclosed entirely from outside either by a thin solid membrane or a thick solid membrane. In a local closed cell cellular structure, each unit cellular structure is individually closed with thick or thin solid membrane at the face and tessellated into design space.

Although recent advances in additive manufacturing (AM) have enabled the fabrication of complex lattice structures, fabricating closed cell lattice structures is challenging and there is no published literature. AM components are generally open cells [8,14–16] because a closed lattice structure possesses the challenge of support structure or support material removal from an enclosed body. It is well known that support material or support structure cannot be removed from an enclosed lattice structure during post-processing without damaging the structure. The material extrusion process is one of the potential technologies to fabricate this closed cell lattice structure with a support-less lattice structure. From this point of view, support-less lattice structures have undiscussed advantages, since they are self-supporting and do not require any support structure during the AM process. Moreover, this extraneous support structure provided during fabrication to avoid the sagging or distortion in the additive manufactured component consumes extra material, time, and energy [17,18]. The current extensively used support-less lattice structure is a honeycomb structure, which is a 2D prismatic structure inspired by nature [7]. This load-bearing structure can be designed and fabricated as a global closed lattice structure using the material extrusion process.

The design of the lattice structure is influenced by three major properties of lattice structure: (1) material properties, (2) topology/shape and unit lattice cell size, (3) lattice structure relative density [10,14]. Two different types of closed cell lattice structures are proposed here: i) local closed cell (see Fig. 1(k)) and ii) global closed cell (see Fig. 1(j)). However, there is no published closed cell lattice structure that is designed and fabricated successfully with any AM processes. Here, a successful closed cell lattice structure fabrication by material extrusion process is shown for the first time. The lattice structures considered here are bio-mimicked structures [19–21] of a sea urchin shape, because they are mechanically stable load-bearing structures [22] with a continuous surface for printing with minimum retraction. The closed lattice structure is obtained as a periodic tessellation of the unit cell, with the concept of closed packing which can be seen in natural materials like bee honeycomb [23].

Here, the local closed cell, global closed cell, and open cell structures are proposed, and the relationship between structural performance and cell size is investigated. Mechanical properties like stiffness and deformation and energy absorption under loading of the local closed cell, global closed cell, and open cell are investigated using numerical and experimental compression testing before benchmarking against typical global closed cell honeycomb lattice [7,10,24]. Scanning electron microscopy (SEM) is also applied to check for sagging or warping of the additively manufactured closed lattice structure.

The results show that the created closed cell lattice structures can be varied covering a wide range of stiffness responses, energy absorption and buckling strength, which can be optimized by analyzing the peculiar damage mechanism.

2. Materials and methods

2.1. Design of close cell lattice structure

In the material extrusion process, designing a closed cell structure must be done with support-less lattice structures. Supports are generally provided when lattice structures have steep overhangs and parallel ledges. Here, the main mechanical property of the closed cell is derived entirely from cell edges or surfaces identical to an open cell lattice structure and thin solid membranes close off the cell faces. Dhruv et al. [21] explained that incorporating lattice structure into design space must follow four steps: 1) design unit lattice (beam type or shell type) based on application, 2) select lattice unit size, 3) select parameter for optimization, and 4) define lattice connectivity in design space. Contemplating these requirements as summarized in Table 1, the closed cell lattice structure designed here results in a surface-based cubic lattice. Load-bearing capacity or energy absorption of the structure depends on how the load is transferred across the lattice. The shape of the unit lattice is designed like a regular sea urchin in the class of Echinoidea (Fig. 1(a)) with a focus on structural morphology as seen in Fig. 1(e). This plate structure is characterized for its remarkable ability to transfer any kind of stress evenly on the surface as seen in the finite element analysis (FEA) simulation in Fig. 2 [25]. The design of urchin or dome type structures is economical in materials because compressive stress is transferred very effectively from the surface of the dome to the urchin margin or ambitus [22,26,27].

FEA is performed to understand the stress distribution across these three structures with no hole, a single hole (sea urchin), and three holes as shown in Fig. 2. The load was applied to the top of the sphere, and the bottom was fixed. Fig. 2(a) shows that the stress is homogenously distributed due to structural symmetry. Force in the solid sphere is divided into a similar component. The curvature changes when a hole is present in the sphere, and the force component is distributed into several components with different magnitudes and directions. In a single hole like in Fig. 2(b), the stress distribution is around the hole with negative curvature. With three holes perpendicular to each other like in Fig. 2(c), large areas with negative curvature are generated. This localizes stress, resulting in a structure that is stiffer with high load-bearing capacity compared to other structures.

The method used for designing the closed cell is based on generating a primitive surface patch defined by boundary curves subject to geometric constraints (Fig. 1(e)). A complete unit cell surface is developed by reflecting the primitive surface across the X = 0, Y = 0, and Z = 0 planes. Here, Matlab© is used to define the boundaries of the primitive surface patch. The boundary equations are applied to the six faces of a primitive cell.

Therefore, if the selected unit lattice size is $2a{\cdot}2a{\cdot}2a$, then the primitive surface patch would be $a{\cdot}a{\cdot}a$. The six curves defined on the six faces of a primitive cell are as follows:

$$\text{Curve 1:@ Z= 0 plane: } (x-a)^2+(y-a)^2=(a/2)^2 \tag{1}$$

$$\text{Curve 2:@ X= a plane: } y^2+z^2=(a/2)^2. \tag{2}$$

$$\text{Curve 3:@ Y= 0 plane: } (z-a)^2+(x-a)^2=(a/2)^2 \tag{3}$$

$$\text{Curve 4:@ Z= a plane: } x^2+y^2=(a/2)^2 \tag{4}$$

$$\text{Curve 5:@ X= 0 plane: } (y-a)^2+(z-a)^2=(a/2)^2 \tag{5}$$

$$\text{Curve 6:@ Y= a plane: } z^2+x^2=(a/2)^2 \tag{6}$$

These six curves constitute the closed boundary of a primitive surface patch. Fig. 1(g) illustrates the upper half of a unit cell obtained

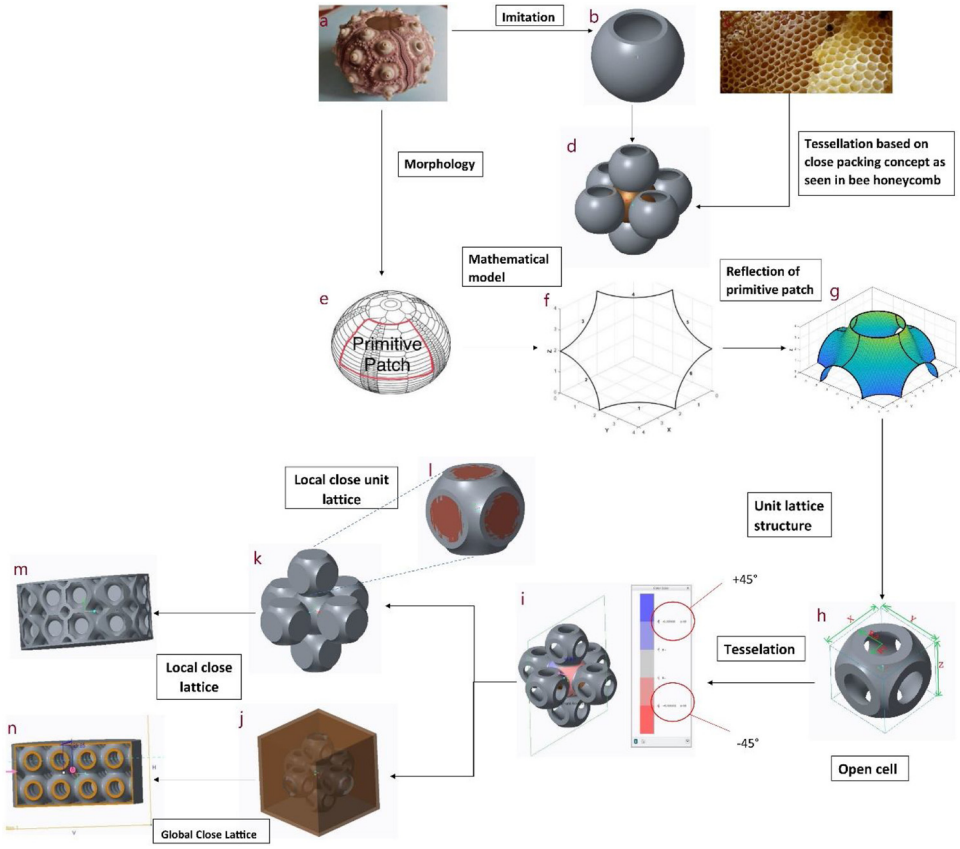

Fig. 1. Design evolution from sea urchin to the support-less closed cell lattice structure.

Table 1
Details of lattice structures designed in this study.

Cell type	Cell size (mm)	No. of cells	Size h_0 (mm)	Shell thickness (mm)	Skin (mm)	ϕ (%)
Open cell 8	8·8·8	4·4·4	32·32·32	1.2	_	32.7
Local closed cell 8	8·8·8	4·4·4	32·32·32	0.6	0.6	32.3
Global closed cell 8	8·8·8	4·4·4	32·32·32	0.66	0.6	32.3
Honeycomb 8	Φ8	5·5·5	32·32·32	0.6	0.6	32.0
Open cell 10.7	10.7·10.7·10.7	3·3·3	32.1·32.1·32.1	1.59	_	32.3
Local closed cell10.7	10.7·10.7·10.7	3·3·3	32.1·32.1·32.1	1.16	0.6	32.3
Global closed cell10.7	10.7·10.7·10.7	3·3·3	32.1·32.1·32.1	0.84	0.6	32.1
Honeycomb	Φ 11	4·4·4	32·32·32	0.9	0.6	31.7

after reflecting the primitive patch across the X = 0 and Y = 0 planes. The generated curves and surfaces were exported into a stereo-lithography (STL) file. Autodesk Fusion 360© & Creo Parametric© was used to mirror, trim, repair and 45° draft checking (Fig. 1(i)) of the SU lattice structure (Fig. 1(h)). Tessellation depends on close packing concept as explained by Pearce [23], so the unit lattice with six faces is surrounded by exactly six lattices in the X, Y, and Z directions and is tightly packed as densely as possible. This type of packing or connection has no remaining void between lattices as seen in Fig. 1(i), reflecting what can be seen also in nature with bee honeycomb or collagenous fiber plate. Hence, this makes tessellation of close lattice as the periodic and unary type with face to face connection in all three directions [21]. Two different types of closed cell lattice structures are designed: 1) local closed cell (Fig. 1(k)(m)) and 2) global closed cell (Fig. 1(j)(n)). The inner radius R_1 and outer radius R_2 are the two important design parameters as seen in Fig. 1(h). The volume reduction coefficient (VRC)

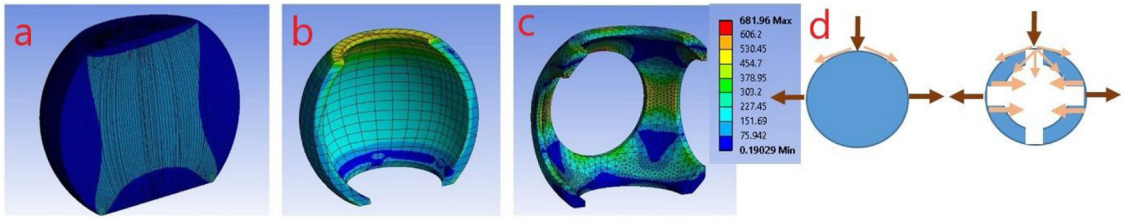

Fig. 2. Stress distribution on sea urchin-inspired structures: a) Solid sphere no hole, b) shell with single hole, and c) shell with three holes. d) Force distribution comparison with solid sphere and spherical shell with three holes.

Table 2
Material extrusion process parameters for printing lattice structures with PLA filament.

Parameters	Value
Print nozzle diameter (mm)	0.4
Nozzle temperature (°C)	205
Bed temperature (°C)	60
Layer height (mm)	0.15
Print infill (%)	100
Print Speed (mm/min)	3500

or relative density Φ are controlled by these radii, while X, Y, and Z control the size of the unit lattice structure:

$$\phi = 1 - \frac{V_L}{V_S} \tag{7}$$

where V_L and V_s are the lattice and solid lattice volumes, respectively.

2.2. Additive manufacturing of lattices

Three specimens of each individual type design reported in Table 1 were fabricated using extrusion process (Flashforge Beaver 3 from Mastech machine co. ltd, Taiwan) after performing the capabilities study of the 3D printer [15,16] with a PLA filament with a 1.75 mm diameter. No special extruder was selected to print this material. The STL file was sliced in the software Simplify3D LLC© version 3.0 with a printing parameter optimized for printing PLA filament listed in Table 2 [29].

These data were uploaded to the 3D printer to fabricate and validate the design. The printing orientation of all the parts is the same as in Fig. 3 with the environment temperature maintained between 20 and 24 °C. No post-processing was done after fabrication, and various designs of support-less lattice structure—both open and closed cells were printed with the same parameters as seen in Table 1.

All lattice structures are fabricated using PLA using color matrix 3D©, Taiwan with a 1.75 mm filament diameter. The reference material properties of PLA are indicated in Table 3.

2.3. Measurements

The surface morphology of the additive manufactured lattice structure was investigated using scanning electron microscopy (SEM) (JEOL JSM-6390LV). Surface defects like distortion or sagging were examined using SEM images. Due to PLA's non-conductive nature, the specimens were subjected to titanium dioxide sputtering on the exposed surface.

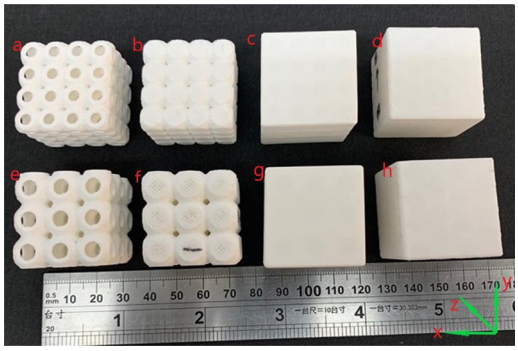

Fig. 3. Fabrication using the material extrusion process: figures (a) and (e) is SU inspired open cell lattice structure with different lattice size, figures (b) and (f) is SU inspired local closed cell lattice structure with different lattice size, figures (c) and (g) SU inspired global closed cell lattice structure with different lattice size, figures (d) and (h) is honeycomb global closed lattice structure with different lattice size. The Z-direction arrow represents the build direction.

Table 3
PLA material properties.

Density (g/cm3)	Young Modulus (MPa)	Tensile stress yield (MPa)	Ultimate tensile strength (MPa)	Poisson's Ratio
1.24	3500	50.5	53.9	0.36

2.4. Compression test

Uniaxial compression tests were performed on all lattice structures with an MTS 810 material test system with a load cell of 100 kN. The compressive displacement was applied at a strain rate of 5 mm/min with displacement up to 40 % of height h_0. The loading direction is perpendicular to print direction for all samples. Load vs. displacement curves were obtained and analyzed. The analysis of the damage and failure mode was performed using visual inspection. Regarding the stress–strain relationships and the energy absorption ability calculation, these quantities are obtained with the following equations [10]:

$$\sigma_{N,c} = \frac{P_c}{A_{0,eq}} \tag{8}$$

$$A_{0,eq} = \frac{V_L}{h_0} = (1 - \phi)h_0^2 \tag{9}$$

$$\varepsilon_{N,c} = \frac{u_c}{h_0} - \tag{10}$$

$$W_c = \int_{\varepsilon=0}^{\varepsilon=\varepsilon_{0.4}} \sigma_{N,c}\varepsilon_{N,c}d\varepsilon \tag{11}$$

where $\sigma_{N,c}$ is the nominal compressive stress, P_c the compressive load, $A_{0,eq}$ an equivalent cross section area of the cell, $\varepsilon_{N,c}$ the nominal compressive strain, u_c the compressive displacement in mm, h_0 the initial cell height, and W_c is the energy absorption per unit volume calculated up to the conventional strain $\varepsilon_{N,c} = 0.4$ due to no stabilized densification strain showed by the tests.

2.5. FE simulation of the mechanical response

A finite element simulation activity was run in parallel with the experimental mechanical tests to corroborate the results and simultaneously test an interactive method of virtual design to predict and optimize the mechanical performances of the lattice structures.

FE models were generated in the ABAQUS/CAE© 2019 code by importing the solid models from the CAE environment and exploiting possible symmetries that were present. Simulations were in the large deformation regime; hence, the non-linear geometry must be optioned. Mesh of solids was done using the ABAQUS automatic algorithm with the inner growth option. Mesh refinement was performed using a convergence analysis of results within the 1% of deviation of the stiffness values. This value was chosen to obtain a good tradeoff between the number of elements and the accuracy due to the complexity of geometries and the nonlinearities of the calculation. Linear solid tetrahedral elements were employed for the same reasons. The resulting number of nodes and elements varied between 10 and 20 thousand and 8 and 14 thousand, respectively, for the ¼ symmetrical geometries.

An isotropic, linear elastic material model was chosen for this study because the aim of the simulation was to first calculate and compare the stiffness of the various structures. However, more complex material models could be used, considering hyper-elasticity, plasticity, or even incorporating PLA damage. Eventual anisotropy due to the material extrusion process, evidenced elsewhere for the same material and process [30,31], can also be modeled. The elastic modulus used in the simulations was selected from literature (Table 3) and optimized to

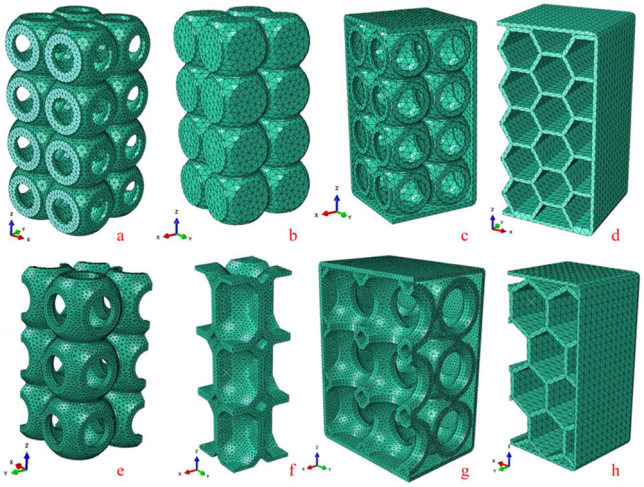

Fig. 4. FE model of lattice structures with reference to the structures *a–h* in Fig. 3.

match the experimental behavior of structures in the elastic regime.

The experiments were simulated by imposing a compression to the lattice by a contact interaction with a rigid analytical surface, where the roughness *small sliding* condition is optioned with a friction coefficient $f = 0.1$. The friction contact was found to fully represent the real test conditions. However, the friction coefficient value was found to not significantly change the results when varying between 0.05 and 0.4. Some of the studied FE models of lattice structures are shown in Fig. 4.

The FE simulation results were elaborated in terms of reaction forces and displacement to obtain the initial stiffness K_0 of the examined structure according to the following relations:

$$F_T = \sum_{i=1}^{N_{C,z}} RF_{z,i} \tag{12}$$

$$K_0 = \frac{dF_T(z)}{dz}\Big|_{(z=0)} \tag{13}$$

where F_T is the total reaction force obtained as the sum of single nodal reaction forces RF_i at the constrained nodes N_C along the z-direction of compression. Before operating the differentiation of Eq. (12), the function $F_T = f(z)$ was regularized by interpolating data points of the FE calculation using a polynomial function of coordinate z over an applied compression strain range of 10–20 %.

3. Results

3.1. SEM analysis

The SEM images of closed cell support-less lattice structure generally show no imperfections like sagging, distortion, or broken lattices within the structure, as seen in Fig. 5. The printed layer is consistent and seems to have a better interaction between the layers, which proves that it is possible to fabricate closed cell lattices with the concept of support-less lattice for the end-user product. This result could help in fabricating load-bearing structures with closed lattice structure which can reduce the manufacturing time and post-processing time, saving a significant amount of material without compromising quality. Furthermore, these lattices are well suited for fabrication based on the extrusion process with a broad range of unit lattice sizes and materials based on application.

3.2. Failure mode of lattice structures

Compression failure modes of closed and open cells with different unit lattice size and morphology are seen in Figs. 6–9. It was found that deformation characteristics of crushed lattice structure fabricated by the material extrusion process depend on the unit lattice structure morphology and are independent of the lattice structure size for the same density.

All three samples of each design show very similar deformation characteristics. The SU lattice structure with both open and closed cells started deforming and collapsing via diagonal shear after fracture of structure as seen in Figs. 6, 8 and 9. The SU local closed cell (Fig. 8) shows a diagonal shear mechanism with double shear bands 45° to the loading direction and finally with layer crushing. This kind of deformation was previously seen with other lattice structure types [32]. The SU global closed cell (Fig. 6) and SU open cell lattice structure (Fig. 9) also started with diagonal shear after fracture [18,19] except the open cell with smaller lattice size of 8 mm started with layer wise deformation and collapsing via local buckling of the bottom layer and subsequently followed by diagonal shear. A similar collapse was also reported by Ketan et al. in skeletal gyroid lattice structures [35]. Global honeycomb closed cell (Fig. 7) deformation started with bottom honeycomb first layer collapse when the critical load was reached. Subsequently, the second layer was reached. This shear failure mode indicates that honeycomb structures are sensitive to bottom layer; a similar trend can also be seen in graded density honeycomb structures [36,37] and in octet truss lattice structures [38].

3.3. Load deformation result

The uniaxial compressive stress–strain curves of all the specimens tested are reported in Fig. 10. Three main deformation regimes were observed [10,33,39]: 1) nearly linear elastic regime marked with red dots; 2) plateau regime which has multiple failure collapse regions, marked with yellow dots; 3) densification regime where the load response rises sharply, marked with green dots. The compressive response of all the cellular lattice structures observed resembles the polymeric lattice structures and foams; the stress–strain curves of all the lattice structures start with linear elastic regime until red dot (1) which is the slope of the line. After the elastic limit (1) the lattice structure starts showing permanent plastic deformation and the onset of local lattice structure buckling, and the curve enters a non-linear regime which indicates plateau regime where sudden decrease of stress is observed until yellow dot point 2. This plateau region is the permanent plastic deformation which happens due to collapse of lattice structure due to buckling. Almost all of the lattice structures show recovery of strength after yellow dot which is the end of plateau regime after sudden drop in the stress. Force is transferred to the second layer, and stress falling suddenly stabilizes. Subsequently, all the layers start buckling with increased stress from point 2 which is also the end of plateau regime and onset of densification. Sudden loss of strength and recovery was seen until all the layer collapsed and started behaving like a solid structure, and this region is the densification region of the lattice structure [13,40,41]. Open cell and local closed cell lattice structures show increasing trend of densification strain and exact densification strain could be beyond the 40 % of deformation. All global closed lattice structure both SU and honeycomb shows local densification after point 2 until green dot which is point 3 and beyond 40 % strain when all the layer collapses could show the exact densification strain.

The initial load–deformation curves of structures are reported in the plot of Fig. 11, where experimental (in black) and FE data (in red) are compared. Results show that FE and experiments are in agreement, even if the PLA Young's modulus has been tuned to 1.8 GPa. Experimental curves generally deviate from linearity quicker than FE, because of the linear material model adopted in simulations. Generally, closed and small-sized cell structures are stiffer than other dispositions, as indicated by Table 4. Here, the error is also calculated, showing that the process of deposition, which is not taken account in the FE models, plays some effects on the elastic stiffness.

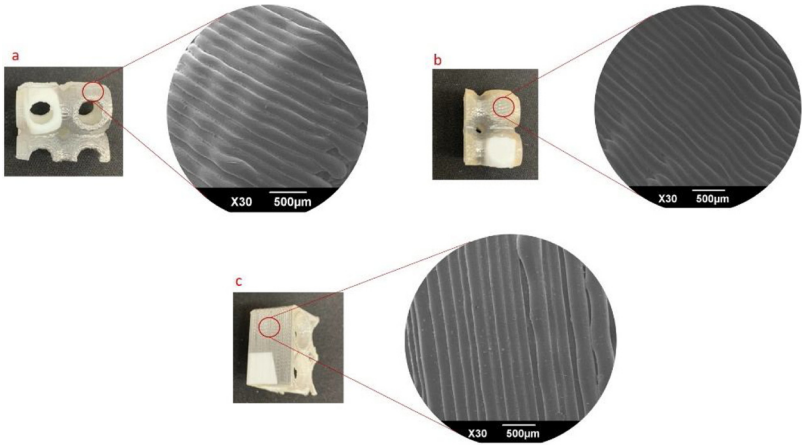

Fig. 5. SEM images of a) open cell lattice structure b) local closed cell lattice structure c) global closed cell lattice structure.

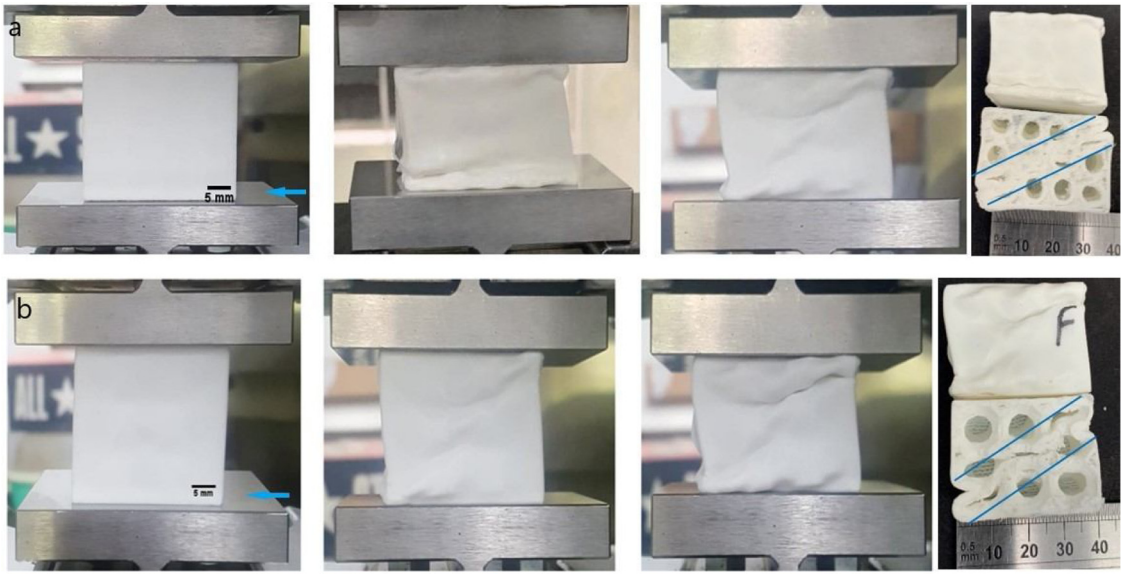

Fig. 6. Experimental compressive deformation of SU global closed cell lattice structures a) cubic cell size 8 mm b) cubic cell size 10.7 mm. The direction of the arrow represents build direction.

Finally, in Fig. 12 the results are plotted in graphical form; as one can notice, again closed small-sized structures reveal better performances in terms of stiffness and energy absorption too.

4. Discussion

Regarding the SU global closed cell structures, it was found that the deformation characteristics are similar for different unit cell sizes because both show a similar trend. Global closed cells deformed and collapsed via diagonal shear after fracture seen in Fig. 10 as a sudden drop in stress was absorbed. This is the plateau region where permanent plastic deformation happens due to structure fracture. The stress started to recover after the sudden drop when, at high strain, the cells collapsed sufficiently so that all the layer combined together to behave like a solid. This steep increased the load, and the structure entered the densification region. In the plateau region, smaller unit cells lost 30 % of their strength compared to 40 % for bigger unit cells. The strength stabilized in the densification region after 25 % total length. Smaller cell lattice structures have better stiffness around 16 % higher than bigger cells for the same density. So smaller cell lattice structures have better mechanical properties in terms of stiffness and better fail-safe design.

The same result is confirmed by elastic FE analysis. As can be seen in Fig. 13, lattice structures *b* and *f* that are smaller in cell size resolve the imposed compressive strain better than other cell structures, open or locally closed, showing a lower strain concentration at the edges. This means that near the initial elastic regime, structures with many, smaller cells distribute the load more efficiently.

In honeycomb global closed cells, it was found that the deformation characteristics were similar for different unit cell sizes because both show a similar trend. Cell buckling started with bottom honeycomb layer collapse when the critical load was reached, which can be seen in Fig. 10 as the sudden drop in the stress is absorbed. The onset of the same mechanism can be seen in FE simulation in Fig. 13 structure *h*. This is the plateau region where plastic deformation happens due to structural fracture The stress started to recover after a sudden drop when at high strain, the cells collapse sufficiently so that all the layers combine together to behave like a solid. This steeply increased the stress, and the structure entered the densification region. In the plateau region, smaller unit cell loses 40 % of strength compared to the bigger unit cell which loses 60 % of its strength and recovers around 80 % of strength in densification region after 30 % deformation. The smaller cell lattice structure has better stiffness, which is around 5.7 % higher than the bigger cell. Therefore, the smaller cell lattice structure has better mechanical properties like stiffness and better fail-safe design.

In the SU open-cell lattice structure, it was found that the

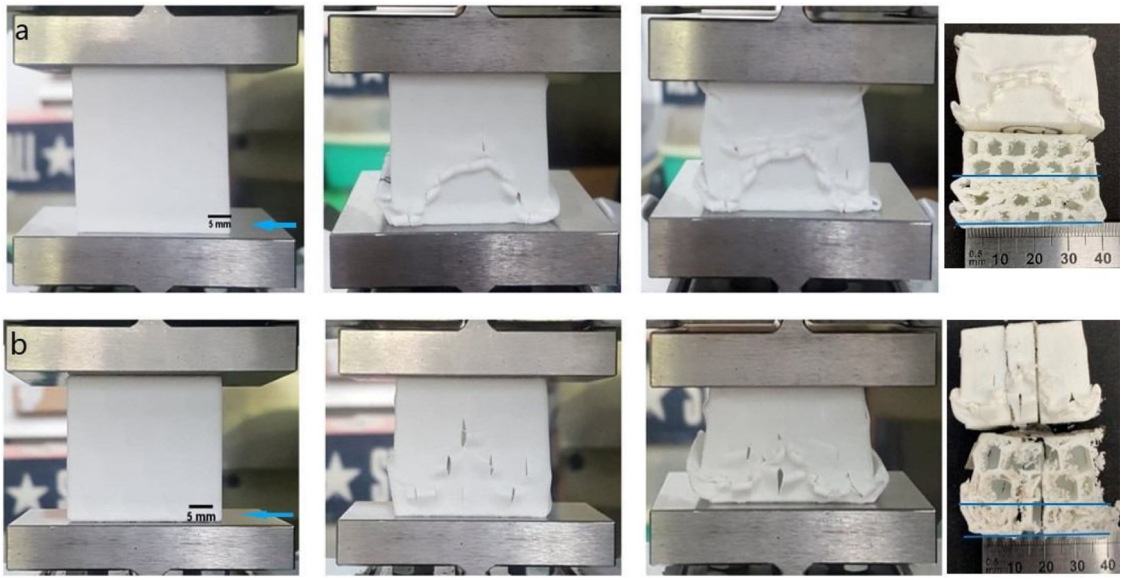

Fig. 7. Experimental compressive deformation of honeycomb global closed cell lattice structures a) cell size 8 mm b) cell size 11 mm. The direction of the arrow represents build direction.

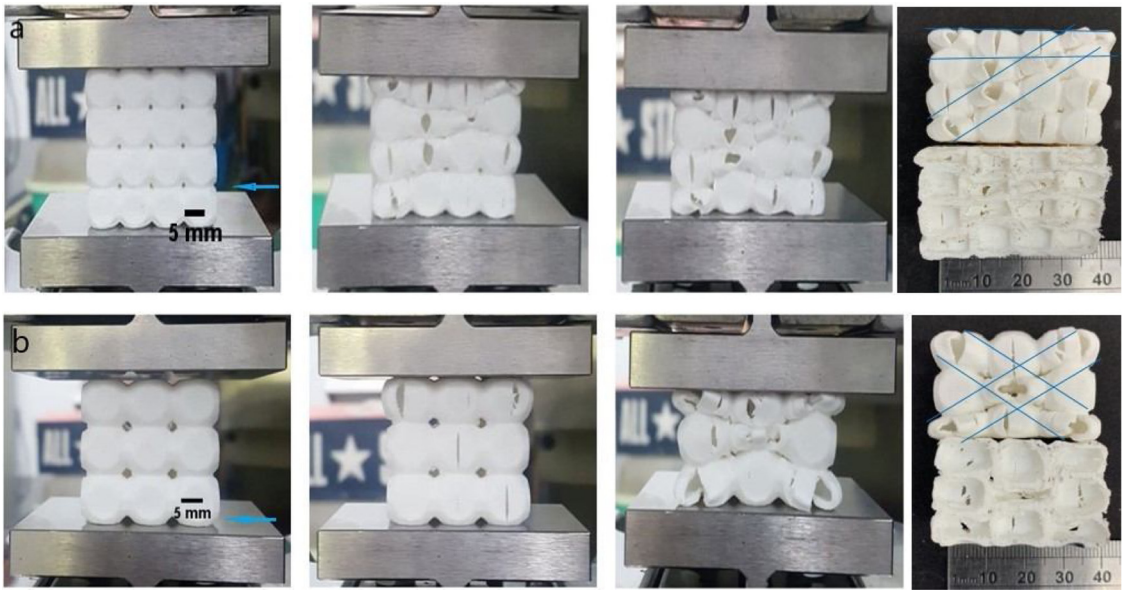

Fig. 8. Experimental compressive deformation of SU local closed cell lattice structures a) cubic cell size 8 mm b) cubic cell size 10.7 mm. The direction of the arrow represents build direction.

deformation characteristics are also almost similar to different unit cell sizes since both deformations are due to diagonal shear. In the plateau region, the smaller unit cells lose 25 % of strength compared to 50 % for bigger cells. Smaller unit cells recover around 80 % of their strength, and bigger cells recover 67 % of strength in the densification region after 40 % deformation of total length. The smaller unit cell lattice structure has better stiffness around 6.5 % higher than bigger cells for the same density. Therefore, the smaller cell lattice structure has better mechanical properties like stiffness and an improved fail-safe design.

In the SU local closed cell, it was found that the deformation characteristics were also nearly the same as diagonal shear failure. This SU local closed cell lattice structure shows very stabilized buckling of cells compared to other cells, resulting in very stable compressive strength rather than a sudden drop. This kind of structure could be safer during load-bearing. In the plateau region, smaller unit cells lost just 10 % of strength compared to 40 % loss of strength for bigger cells. They suddenly began recovering after 30 % deformation of total length. Nearly the same strength was gained after 40 % of deformation, while the bigger cell gained 70 % of its strength. Smaller cell lattice structures have better stiffness around 6.5 % higher than bigger cells for the same density. Therefore, smaller cell SU close cell lattice structures have better mechanical properties like stiffness, energy absorption and better fail-safe design compared to all the lattice structures tested here. This was followed by the SU global close cell lattice structure. It is also clear from the compressive and FE simulation that smaller cell size of same density plays an important role in mechanical properties. Smaller cell has high resistance to buckling as slenderness decreases and arrest a crack prorogation which improves the stiffness of load bearing structure and has minimum effect on manufacturing related defects.

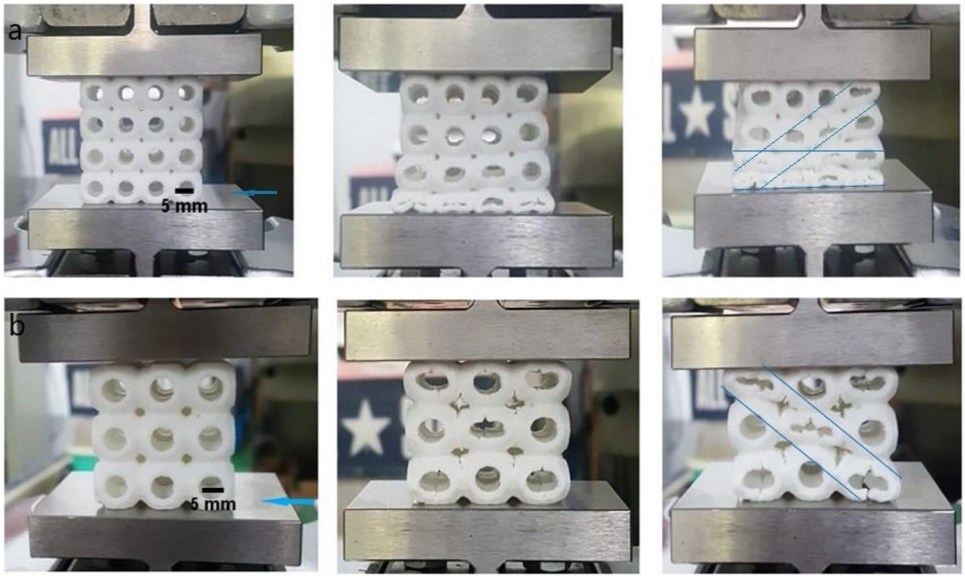

Fig. 9. Experimental compressive deformation of SU open cell lattice structures a) cubic cell size 8 mm b) cubic cell size 10.7 mm. The direction of the arrow represents build direction.

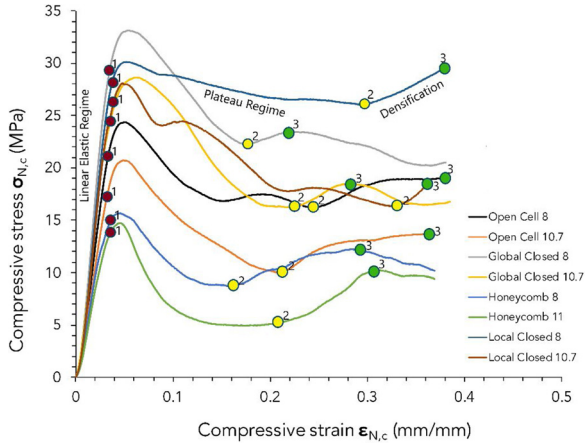

Fig. 10. Experimental stress-strain curves of the compression tests on the lattice structures with the same density and different unit cell sizes.

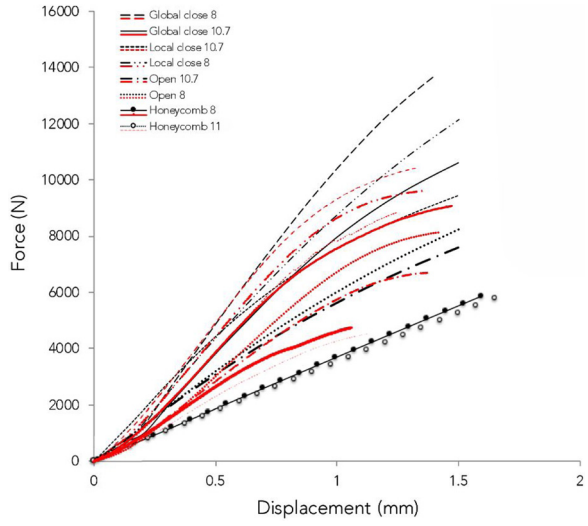

Fig. 11. FE and experimental curves in the elastic regime (black: experimental; red: simulation).

5. Conclusions

This study evaluates the design and manufacturability of closed cell lattice structures with PLA filaments and material extrusion processes for application in load-bearing structures. Closed cell lattice structures were designed with the concept of support-less lattice structures, which is shell type, bio-mimicked and inspired by sea urchins. This periodic closed cell lattice structure offers great potential for fabrication parts with a wide range of volume fraction/density and different unit cell sizes, reducing the material, energy consumption, and production because it has high load-bearing capacity compared to open cell. Also, no post-processing is involved to remove the support from the lattice.

Closed cell lattice structures also have a design advantage because they show strong load-bearing capacity compared to open cell lattice structures, and can be encapsulated with a fluid or pressurized air to provide strength and damping characteristics. Other relevant findings can be summarized as follows:

1 SEM results demonstrate that closed cell lattice structures can be fabricated with the material extrusion process since no imperfections like sagging, distortion, or breaking were observed in the close cell lattice structures;
2 the cell size of same density has an important role for load-bearing structures since all samples of different designs showed that smaller cell size has better stiffness and fail-safe design due to improved resistance to buckling;
3 the same holds for the load-bearing structure application, since the SU local closed cell lattice structure with small cell size gave high strength, high energy absorption and fail-safe design compared to the open cell or global closed cell structures;
4 in particular, SU local closed cell has almost the same stiffness as SU global close cell, but it was 46 % higher and 25 % higher compared to benchmarked honeycomb and open cell lattice structures, respectively.

Author disclosure statement

"No competing financial interests exist." The design of a sea urchin closed cell lattice structure is applied for United states patent and trademark office and Taiwan patent.

Table 4
Mechanical properties of lattice structures.

Cell structure	Experimental stiffness (N/mm)	FE simulation (N/mm)	Δ (%)	Experimental Elastic limit (MPa)	Experimental Energy absorbed Wc (MJ/m^3)
Open cell 8	7059	7336	+3.9 %	21.1	6.8
Open cell 10.7	5739	6051	+5.4 %	17.2	4.8
Global closed cell 8	9716	8582	−11.7 %	29.3	9.0
Global closed cell 10.7	7940	8456	+6.5 %	24.0	7.4
Local closed 8	9351	9395	+0.5 %	28.2	10.0
Local closed 10.7	8743	8547	−2.2 %	26.2	7.1
Honeycomb 8	5043	4951	−1.8 %	15.4	4.0
Honeycomb 11	4770	4861	+1.9 %	14.5	2.9

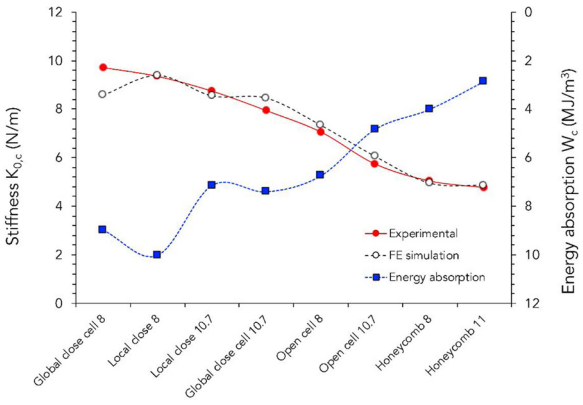

Fig. 12. FE and experimental stiffness and the experimental energy absorbed per unit volume of lattice structures.

Note

The design of closed cell lattice structure has been applied for United States Patent and Trademark Office and Taiwan Patent.

CRediT authorship contribution statement

Ajeet Kumar: Conceptualization, Methodology, Investigation, Writing - original draft. **Luca Collini:** Validation, Formal analysis, Writing - review & editing. **Alix Daurel:** Data curation, Investigation. **Jeng-Ywan Jeng:** Resources, Project administration, Supervision.

Declaration of Competing Interest

The authors declare that they have no known competing financial interests or personal relationships that could have appeared to influence the work reported in this paper.

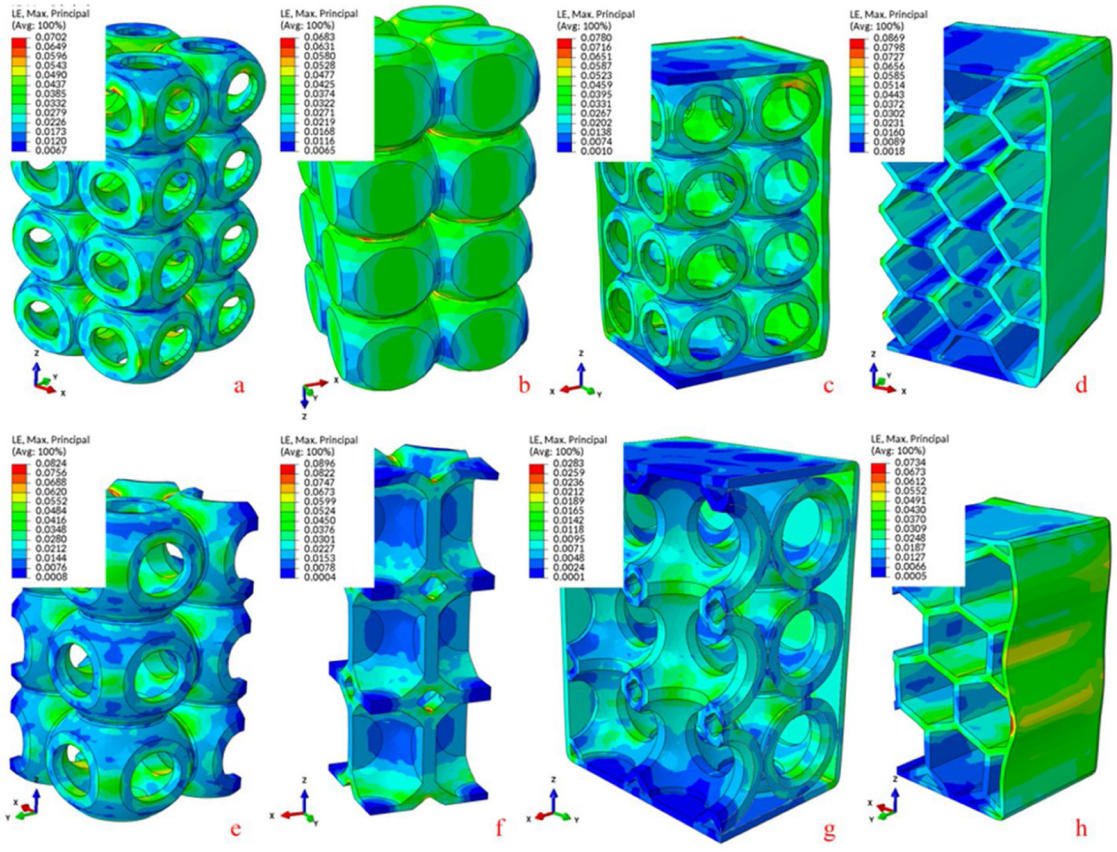

Fig. 13. Maximum strain distribution in the lattice structures under 5% of compression.

Acknowledgments

This work was financially supported by the High Speed 3D Printing Research Center from the Featured Areas Research Center Program within the framework of the Higher Education Sprout Project by the Minister of Education (MOE) (grant number 108PO12) in Taiwan.

References

[1] T. Wester, Nature teaching structures, Int. J. Space Struct. 17 (2–3) (2002) 135–147, https://doi.org/10.1260/026635102320321789.
[2] C. Tavsan, F. Tavsan, E. Sonmez, Biomimicry in architectural design education, Procedia Soc. Behav. Sci. 182 (2015) 489–496, https://doi.org/10.1016/j.sbspro.2015.04.832.
[3] Y. Helfman Cohen, Y. Reich, S. Greenberg, Biomimetics: structure–function patterns approach, J. Mech. Des. 136 (2014) 111108, , https://doi.org/10.1115/1.4028169.
[4] M.S. Aziz, A.Y. El Sherif, Biomimicry as an approach for bio-inspired structure with the aid of computation, Alexandria Eng. J. 55 (2016) 707–714, https://doi.org/10.1016/j.aej.2015.10.015.
[5] S. Arslan, A. Sorguc, Similarities between Structures in Nature and Man-Made Structures : Biomimesis in Architecture 73 WIT Press, 2004, pp. 45–54 Des Nat II Comp Des Nat with Sci Eng..
[6] Z. Qin, B.G. Compton, J.A. Lewis, M.J. Buehler, Structural optimization of 3D-printed synthetic spider webs for high strength, Nat. Commun. 6 (2015) 1–7, https://doi.org/10.1038/ncomms8038.
[7] Q. Zhang, X. Yang, P. Li, G. Huang, S. Feng, C. Shen, B. Han, X. Zhang, F. Jin, F. Xu, T.J. Lu, Bioinspired engineering of honeycomb structure – using nature to inspire human innovation, Prog. Mater. Sci. 74 (2015) 332–400, https://doi.org/10.1016/j.pmatsci.2015.05.001.
[8] A. Nazir, K.M. Abate, A. Kumar, J.-Y. Jeng, A state-of-the-art review on types, design, optimization, and additive manufacturing of cellular structures, Int. J. Adv. Manuf. Technol. 104 (3489) (2019) 3489–3510, https://doi.org/10.1007/s00170-019-04085-3.
[9] T. Mcnulty, D. Bhate, A. Zhang, M.A. Kiser, L. Ferry, A. Suder, S. Bhattacharya, P. Boradkar, A framework for the design of biomimetic cellular materials for additive manufacturing, Solid Freeform Fabr. Symp. (2017) 2188–2200.
[10] L.J. Gibson, M.F. Ashby, Cellular Solids: Structure and Properties, Cambridge University Press, 1999.
[11] A. Nazir, K.M. Abate, A. Kumar, J.Y. Jeng, A state-of-the-art review on types, design, optimization, and additive manufacturing of cellular structures, Int. J. Adv. Manuf. Technol. 104 (2019) 3489–3510, https://doi.org/10.1007/s00170-019-04085-3.
[12] M.M.J. Opgenoord, K.E. Willcox, Design for additive manufacturing: cellular structures in early-stage aerospace design, Struct. Multidiscipl. Optim. 60 (2019) 411–428, https://doi.org/10.1007/s00158-019-02305-8.
[13] M.F. Ashby, The properties of foams and lattices, Philos. Trans. R. Soc. A Math. Phys. Eng. Sci. 364 (2006) 15–30, https://doi.org/10.1098/rsta.2005.1678.
[14] C. Beyer, D. Figueroa, Design and analysis of lattice structures for additive manufacturing, J. Manuf. Sci. Eng. 138 (2016) 121014, , https://doi.org/10.1115/1.4033957.
[15] W. Tao, M.C. Leu, Design of lattice structure for additive manufacturing, Int. Symp. Flex. Autom. (2016) (2016) 1–3.
[16] A. Takezawa, K. Yonekura, Y. Koizumi, X. Zhang, M. Kitamura, Isotropic Ti–6Al–4V lattice via topology optimization and electron-beam melting, Addit. Manuf. 22 (2018) 634–642, https://doi.org/10.1016/j.addma.2018.06.008.
[17] A.T. Gaynor, J.K. Guest, Topology optimization considering overhang constraints: eliminating sacrificial support material in additive manufacturing through design, Struct. Multidiscipl. Optim. 54 (2016) 1157–1172, https://doi.org/10.1007/s00158-016-1551-x.
[18] A. Kumar, S. Verma, J. Jeng, Supportless lattice structures for energy absorption fabricated by fused deposition modeling, 3D Print. Addit. Manuf. (2020), https://doi.org/10.1089/3dp.2019.0089 In press.
[19] A. du Plessis, C. Broeckhoven, I. Yadroitsava, I. Yadroitsev, C.H. Hands, R. Kunju, D. Bhate, Beautiful and functional: a review of biomimetic design in additive manufacturing, Addit. Manuf. 27 (2019) 408–427, https://doi.org/10.1016/j.addma.2019.03.033.
[20] A. du Plessis, C. Broeckhoven, I. Yadroitsev, I. Yadroitsava, S.G. le Roux, Analyzing nature's protective design: the glyptodont body armor, J. Mech. Behav. Biomed. Mater. 82 (2018) 218–223, https://doi.org/10.1016/j.jmbbm.2018.03.037.
[21] D. Bhate, C.A. Penick, L.A. Ferry, C. Lee, Classification and selection of cellular materials in mechanical design: engineering and biomimetic approaches, Designs 3 (2019) 19, https://doi.org/10.3390/designs3010019.
[22] T. Malcolm, Domes, arches and urchins: the skeletal architecture of echinoids (Echinodermata), Zoomorphology 105 (1985) 114–124, https://doi.org/10.1007/BF00312146.
[23] P. Pearce, Structure in Nature is a Strategy for Design, The MIT Press, Cambridge, MA, USA, 1990.
[24] P. Hao, J. Du, Energy absorption characteristics of bio-inspired honeycomb column thin-walled structure under impact loading, J. Mech. Behav. Biomed. Mater. 79 (2018) 301–308, https://doi.org/10.1016/j.jmbbm.2018.01.001.
[25] S.M. Sajadi, P.S. Owuor, S. Schara, C.F. Woellner, V. Rodrigues, R. Vajtai, J. Lou, D.S. Galvão, C.S. Tiwary, P.M. Ajayan, Multiscale geometric design principles applied to 3D printed schwarzites, Adv Mater. 30 (2018) 1704820, , https://doi.org/10.1002/adma.201704820.
[26] O. Ellers, A mechanical model of growth in regular sea urchins: predictions of shape and a developmental morphospace, Proc. R. Soc. Lond. Ser. B Biol. Sci. 254 (1993) 123–129, https://doi.org/10.1098/rspb.1993.0136.
[27] T. Wester, A geodesic dome-type based on pure plate action, Int. J. Space Struct. 5 (1990) 155–167, https://doi.org/10.1177/026635119000500302.
[29] G. Dong, G. Wijaya, Y. Tang, Y.F. Zhao, Optimizing process parameters of fused deposition modeling by Taguchi method for the fabrication of lattice structures, Addit. Manuf. 19 (2018) 62–72, https://doi.org/10.1016/j.addma.2017.11.004.
[30] Y. Zhao, Y. Chen, Y. Zhou, Novel mechanical models of tensile strength and elastic property of FDM AM PLA materials: experimental and theoretical analyses, Mater. Des. 181 (2019) 108089, , https://doi.org/10.1016/j.matdes.2019.108089.
[31] R. Zou, Y. Xia, S. Liu, P. Hu, W. Hou, Q. Hu, C. Shan, Isotropic and anisotropic elasticity and yielding of 3D printed material, Compos. Part B Eng. 99 (2016) 506–513, https://doi.org/10.1016/j.compositesb.2016.06.009.
[32] L. Zhang, S. Feih, S. Daynes, S. Chang, M.Y. Wang, J. Wei, W.F. Lu, Energy absorption characteristics of metallic triply periodic minimal surface sheet structures under compressive loading, Addit. Manuf. 23 (2018) 505–515, https://doi.org/10.1016/j.addma.2018.08.007.
[33] S.Y. Choy, C.N. Sun, K.F. Leong, J. Wei, Compressive properties of functionally graded lattice structures manufactured by selective laser melting, Mater. Des. 131 (2017) 112–120, https://doi.org/10.1016/j.matdes.2017.06.006.
[35] O. Al-Ketan, R. Rowshan, R.K. Abu Al-Rub, Topology-mechanical property relationship of 3D printed strut, skeletal, and sheet based periodic metallic cellular materials, Addit. Manuf. 19 (2018) 167–183, https://doi.org/10.1016/j.addma.2017.12.006.
[36] S.R.G. Bates, I.R. Farrow, R.S. Trask, Compressive behaviour of 3D printed thermoplastic polyurethane honeycombs with graded densities, Mater. Des. 162 (2019) 130–142, https://doi.org/10.1016/j.matdes.2018.11.019.
[37] P. Zhang, D.J. Arceneaux, A. Khattab, Mechanical properties of 3D printed polycaprolactone honeycomb structure, J. Appl. Polym. Sci. 135 (2018), https://doi.org/10.1002/app.46018.
[38] M. Mohsenizadeh, F. Gasbarri, M. Munther, A. Beheshti, K. Davami, Additively-manufactured lightweight Metamaterials for energy absorption, Mater. Des. 139 (2018) 521–530, https://doi.org/10.1016/j.matdes.2017.11.037.
[39] T. Maconachie, M. Leary, B. Lozanovski, X. Zhang, M. Qian, O. Faruque, M. Brandt, SLM lattice structures: properties, performance, applications and challenges, Mater. Des. 183 (2019), https://doi.org/10.1016/j.matdes.2019.108137.
[40] I. Maskery, N. Aboulkhair, A. Aremu, C. Tuck, I. Ashcroft, Compressive failure modes and energy absorption in additively manufactured double gyroid lattices, Addit. Manuf. 16 (2017) 24–29, https://doi.org/10.1016/j.addma.2017.04.003.
[41] P.B. Su, B. Han, M. Yang, Z.H. Wei, Z.Y. Zhao, Q.C. Zhang, Q. Zhang, K.K. Qin, T.J. Lu, Axial compressive collapse of ultralight corrugated sandwich cylindrical shells, Mater. Des. 160 (2018) 325–337, https://doi.org/10.1016/j.matdes.2018.09.034.